ELSEVIER

Cement & Concrete Composites 25 (2003) 351–356

Cement & Concrete Composites

www.elsevier.com/locate/cemconcomp

Electrical effects generated by mechanical loading of hardened Portland cement paste

M. Cabeza, P. Merino, X.R. Nóvoa *, I. Sánchez

Universidade de Vigo, E.T.S.E.I., Lagoas-Marcosende 9, 36200 Vigo, Spain

Accepted 22 July 2002

Abstract

This work presents results on the effect of applied load on the electrical properties (resistivity and capacitance) of hardened cement paste. Impedance spectroscopy measurements in the high frequency region (100 kHz–15 MHz) show two time constants, one associated to the solid phase, and the other to the liquid filling the pores. The time constant associated with the liquid phase is sensitive to external loads acting on the specimen. The observed variations are explained in terms of electrolyte drag from interlaminar spaces and structure pores and vice versa. The importance of those electrolyte movements concerning structure fatigue and rebars corrosion is also discussed.

Keywords: Cement pastes; Impedance spectroscopy; Load; Creep; Microstructure

1. Introduction

The use of electrical parameters as a diagnostic tool in cement and concrete research has a long history [1] and simple resistive electrical models have been employed to correlate microstructure and concrete's response. Resistivity measurements are carried out at a fixed frequency (usually in the 100 Hz–10 kHz range, to avoid interfacial effects) and the resistance measured is assumed to be attributed primarily to ionic conduction effects through continuous electrolyte-filled capillary pores within the bulk material. The importance of frequency on electrical measurements in cement and concrete has been highlighted since the early 1990s [2,3] and attempts have been made to correlate impedance spectroscopy data and pore size distribution [4].

The high frequency capacitive loop observed in the 100 kHz–100 MHz frequency range (Fig. 1, triangles) has been interpreted in terms of a "dielectric amplification factor" linked to concrete microstructure [5–8]. More recently other works [9–11] demonstrated that two time constants are present in the above-mentioned capacitive loop, one of them associated to the solid matrix and the other one to ionic motion in the solution filling the pores. This result was achieved by separation of interfacial and bulk contributions either using a polymeric sheet [9,10] or an air gap [11] to avoid any physical contact between electrodes employed for applying the electric field and the tested sample. The shape of the impedance spectra obtained in this way corresponds to the data in Fig. 1 (cross symbols).

The absence of contact between the electrodes and the tested sample reduces the contributions to the overall impedance to the response of the electrolyte filling the pores plus the bulk material. Any dc paths crossing the sample and give rise to electrochemical processes at electrodes are avoided. The physical model as well as its electrical equivalent were presented in [11] and have been adapted to give Fig. 2. The capacitance C_1 corresponds to the dielectric contribution of the solid phase, and the R_2C_2 time constant shall correspond to ionic motion in the liquid phase [10].

The correlation between C_1 and the solid phase fraction has also been established in hardened cement paste [12,13] using mercury intrusion porosimetry that gives a direct evaluation of the sample's porosity (and pore size distribution), in spite of the inherent limitations of the method [14].

* Corresponding author. Tel.: +34-986-812-213; fax.: +34-986-812-201.

E-mail address: rnovoa@uvigo.es (X.R. Nóvoa).

0958-9465/03/$ - see front matter
PII: S0958-9465(02)00053-7

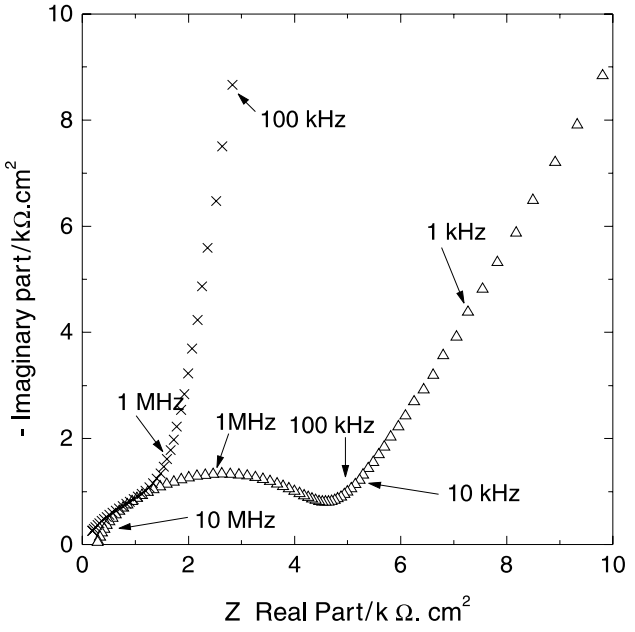

Fig. 1. Nyquist plots corresponding to the impedance spectra obtained from damp hardened cement paste using direct contact between the sensing electrodes and the cement paste (triangles) and after interfacial effects elimination (crosses).

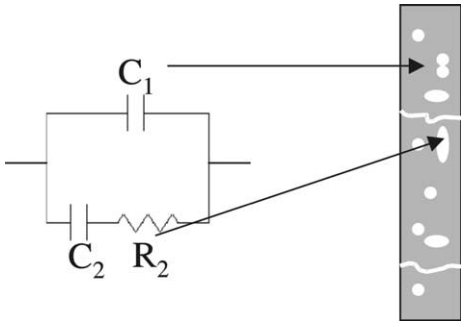

Fig. 2. Cement paste model and electrical equivalent circuit (adapted from [11]).

This work is intended to give an insight to the R_2C_2 time constant analysing its relationship with load applied to the studied probe.

2. Experimental

2.1. Sample preparation

Portland cement (CEM I 52.5R) was employed for cement paste preparation using water to cement ratio (w/c) = 0.4. The nominal composition (wt.%) of the employed cement is: CaO 62.5%, SiO_2 21.0%, Al_2O_3 6.5%, Fe_2O_3 2.5%, MgO 2.0%, SO_3 2%, ($K_2O + Na_2O$) 0.5%.

After mechanical mixing, the mixture was cast into a cylindrical mould (5.9 cm in diameter and 20 cm high) and hand tamped to minimise air voids. The cylinder, demoulded after two days, was held at 100% RH for 28 days. At that age, slices having different thickness were wet cut from the cylinder using a diamond-blade saw. Those slices were checked for face planarity and parallel alignment to ±0.2 mm as well as for eye visible defects/voids. Only samples passing those verifications were returned to the humidity chamber, waiting for the impedance measurements to be performed.

2.2. Impedance measurements and data processing

Impedance spectra were obtained using a HP4194A impedance/gain-phase analyser that allows capacitance measurements in the range 10^{-14}–10^{-1} F having a maximum resolution of 10^{-16} F. The impedance spectra were obtained in purely AC mode using 100 mV rms amplitude signal in the 10 kHz–15 MHz frequency range. In order to avoid/minimise the possible contributions due to the electrode–sample interface, two different measuring methods have been employed.

The measurements performed under applied load have been conducted using the experimental arrangement schematically depicted in Fig. 3. The sample was loaded using a clamp incorporating a stress transducer that allows direct reading of the step-by-step applied load. The manually driven clamp acts on two copper electrodes ($\phi = 4$ cm) covered by a graphite sheet (high density, nuclear grade) on the sample's side. Two polyester sheets (100 μm thick) ionically isolate the sample and the electric field driving electrodes. The contribution of these polyester sheets is numerically removed from the bulk data. This procedure was already employed in a previous work [9].

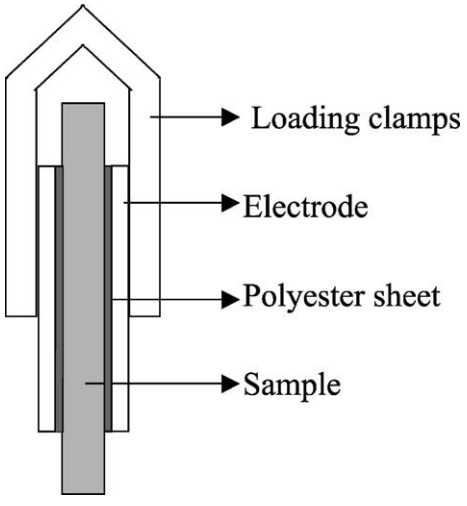

Fig. 3. Cell employed for impedance measurements (schematic).

For the impedance measurement without load applied, a non-contacting electrode [11] leaving an air gap of 100 μm at each side of the sample was used. This method served also as a reference to verify that the contribution of the polyester sheets was correctly eliminated in the contacting method, and also to validate the self-consistence and reproducibility of the measurements by using the sample's thickness as a normalising parameter. The procedure has been described in recent publications [11,13].

Once the rough experimental impedance data were corrected for the polyester or air gap contributions, a minimisation procedure based in a simplex method [9] was conducted in order to obtain the relevant parameters corresponding to the chosen equivalent electrical model (Fig. 2).

3. Results and discussion

The data depicted in Fig. 4a correspond to a typical Nyquist impedance plot obtained after removing the contribution of the air gap or polyester sheet (depending on the measuring method). The feature is capacitive so it is interesting to work in the complex capacitance plane using Cole–Cole representations. Fig. 4b corresponds to the Cole–Cole representation of data given in Fig. 4a. The numerical transformation was conducted using Eq. (1).

$$C^*(\omega) = \frac{1}{j\omega Z(\omega)} \tag{1}$$

where $C^*(\omega)$ represents the complex capacitance at angular frequency ω, $Z(\omega)$ the measured impedance at ω, $\omega = 2\pi f$, and $j = (-1)^{1/2}$.

$$C^*(\omega) = C_1 + \frac{C_2}{(1 + (j\omega R_2 C_2)^{\alpha})^{\beta}} \tag{2}$$

Eq. (2) has the advantage of showing two well-defined limits at high and low frequency in the complex plane capacitance plot (Fig. 4b), respectively C_1 and $C_1 + C_2$. Additionally, it is easy to take account of the R_2C_2 time constant dispersion. The Havriliak–Negami formalism [15] has been employed for this purpose. α and β parameters in Eq. (2) are constants, $0 < \alpha$, $\beta \leqslant 1$, that account respectively for the symmetric (Cole–Cole) and asymmetric (Cole–Davidson) dispersion of the R_2C_2 time constant. The possible relationship between cement paste microstructure and α and β parameters will be discussed elsewhere. The discussion here is focussed on the "electrical" parameters R_2 and C_2.

The capacitance data given in Fig. 4b show that the chosen model is able to reproduce properly the experimental data. The resulting C_1 and C_2 parameters are plotted in Fig. 5 as a function of sample thickness. It can be seen that while the high frequency capacitance, C_1, scales correctly with sample thickness (according to

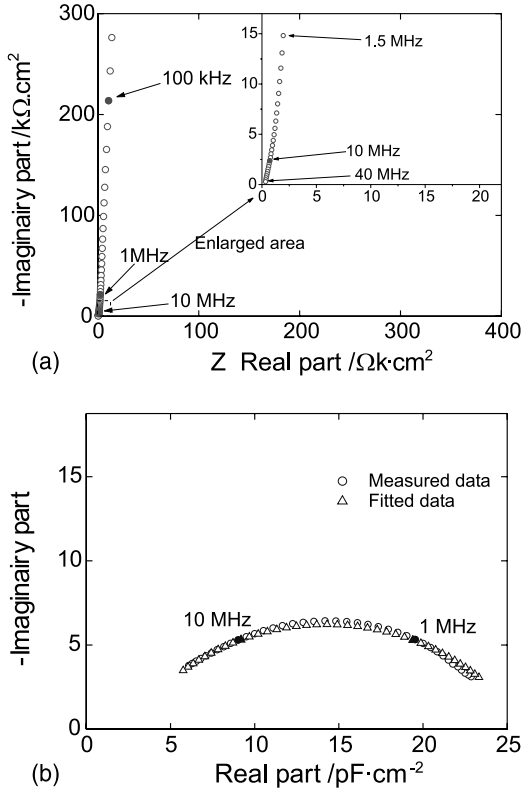

Fig. 4. (a) Nyquist plot corresponding to the impedance data obtained for a w:c = 0.4 sample after 34 days ageing. Sample thickness = 0.78 cm. (b) Cole–Cole plot corresponding (circles) to impedance data given in Fig. 4a (according to Eq. (1)). Triangle-shaped symbols correspond to fitted data using the equivalent circuit given in Fig. 2. The best fitting parameters, described in Eq. (2) are C_1: 0.97 pF cm^{-2}, R_2: 4.41 kΩ cm^2, C_2: 29.88 pF cm^{-2}, α: 0.75, β: 0.58.

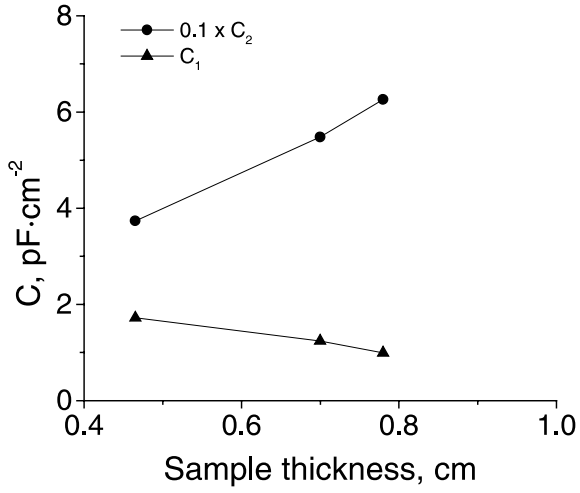

Fig. 5. Dependence of C_1 and C_2 parameters on sample thickness at constant applied load (74 kPa).

Eq. (3) for the capacitance of a flat condenser), C_2 increases with sample thickness.

$$C = \varepsilon\varepsilon_0 \frac{S}{d} \tag{3}$$

In Eq. (3), C accounts for the capacitance of a flat condenser (F), ε for the relative dielectric constant of the dielectric between electrodes, ε_0 for the vacuum permittivity (8.85×10^{-14} F cm^{-1}), and S and d are respectively the electrode area (cm^2) and the distance between electrodes (cm).

Eq. (3) and C_1 data in Fig. 5 allow obtaining the apparent dielectric constant value $\varepsilon \approx 9$ for this type of cement and water-to-cement ratio. This value is not dependent on the applied load or on the amount of water in the sample [16].

According to the proposed model the R_2C_2 time constant is associated to the ionic motion in the liquid phase. This idea was already advanced in previous papers [10,11] however the results obtained were never discussed in depth because it was not possible to find any correlation with external variables.

Classical textbooks [17] refer that if concrete is placed under a sustained compressive load, then creep will occur. Concrete deformation can be originated both by load creep and drying shrinkage. The major difference between shrinkage and creep is that the first one is associated with the removal of adsorbed water to the atmosphere, whereas the latter is considered to be due to its movement within the concrete [18]. Several mechanisms have been proposed to explain creep [19] but, in some way, most of them agree that the movement of physically adsorbed water on the C–S–H gel particles plays an important role.

Recent data [19] suggest that slipping and sliding processes involving C–S–H gel sheets are also associated to the creeping process, so explaining the microstructural changes associated to creep.

According to the above reviewed concepts, creep causes interlaminar water to move away towards the

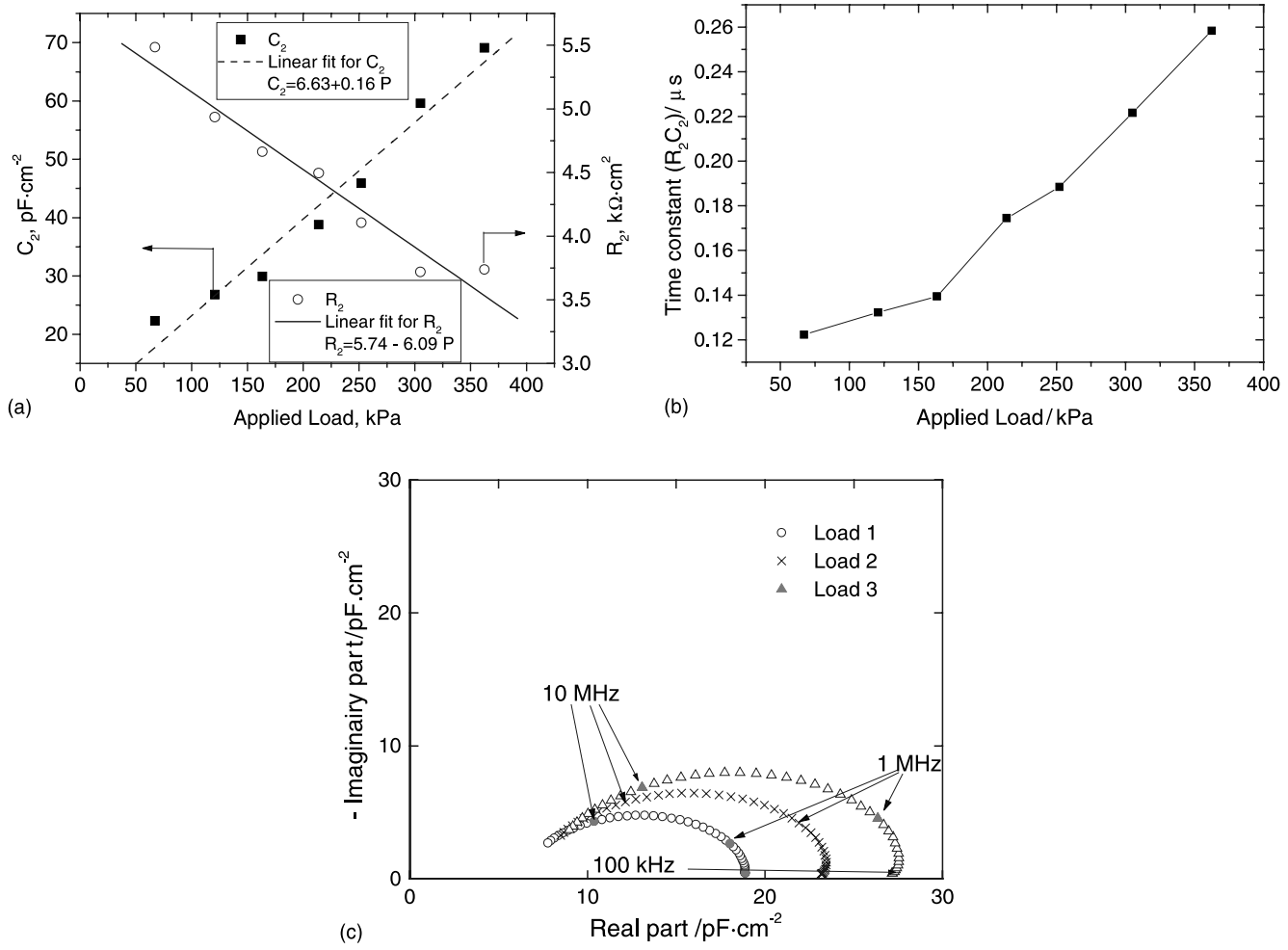

Fig. 6. (a) Dependence of R_2 and C_2 parameters on applied load. Sample thickness = 0.7 cm, 70 days hardening. (b) Dependence of the time constant $\tau_2 = R_2C_2$ on applied load (R_2 and C_2 data from Fig. 6a). (c) Dependence of the complex capacitance on mechanical load applied to a 0.4 cm thick sample. The phase rotation associated to τ_2 variation is indicated. Load 1, 2, 3 are respectively 25, 50 and 75 kPa.

unoccupied spaces (pores) in hardened cement paste. The water so liberated will dissolve ions from pore walls and will increase the total amount of electrolyte in pores and thus, the bulk cement paste resistivity will be decreased. The results depicted in Fig. 6a are consistent with this hypothesis because the R_2 parameter decreases linearly as applied load increases. Additionally, if the electrolyte filling the pores is considered as a space charge region, the C_2 parameter is directly proportional to the total amount of ionic charges present, i.e., the amount of electrolyte. Thus, its value shall increase as applied load does, and this is the behaviour observed in Fig. 6a and c.

According to Fig. 6a, the dependence of C_2 parameter on applied load is about twice that obtained for R_2. This means that the R_2C_2 time constant is load dependent. Fig. 6b summarises this dependence. The above referred slipping and sliding processes involving C–S–H gel sheets [19] can help in the understanding of this variation. The ionic motion induced by the applied electric field shall have a time constant $R_2C_2 = \delta^2/D$ [10] where δ represents the effective path distance (pore diameter) and D the average diffusion coefficient of the ionic species involved (OH^-, Na^+, K^+, Ca^{2+}, ...). The diffusion coefficient of the different ionic species is concentration dependent, but remaining in the 10^{-5} $cm^2\,s^{-1}$ range. So, taken $D \approx 10^{-5}$ $cm^2\,s^{-1}$, the data depicted in Fig. 6b indicate that the effective path distance increases from 10 to 16 nm as load is increased from 50 to about 400 kPa. It seems that small pores increase their connectivity, probably due to slipping and sliding processes involving C–S–H gel sheets and/or microcrack formation. Microcrack formation has been considered to interpret electrical effects observed in mortars under low-level load [20,21]. Moreover, a time constant for ionic mobility in gel pores has already been introduced to understand high frequency impedance spectra obtained on cement-based materials [22].

Some hypotheses reviewed in the literature [19] claim that smallest pores dominate the creep characteristics and here an average diameter of 13 nm is obtained. In order to verify this aspect, some pore size determinations have been performed using mercury intrusion porosimetry. The results depicted in Fig. 7 are in good agreement with this hypothesis and the impedance results. The smallest pore diameter is about 15 nm, so the R_2C_2 time constant corresponds to the electrolyte filling those pores.

The load range employed in this study was 10–20 times lower than the usually employed in creep tests. The reasons for this choice were twofold. First, it was intended to develop a method able to detect small load variations and secondly, it was the aim of keeping in the linear and reversible region of the strain–time curve in order to perform cyclic measurements. Information concerning microstructural modifications under cyclic low loading has already been obtained by dc electrical resistivity measurements [20].

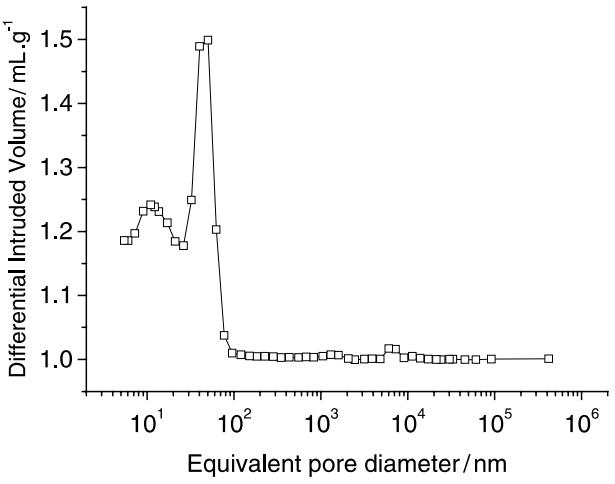

Fig. 7. Pore size distribution obtained by mercury intrusion porosimetry on a sample of 0.4 w:c ratio at 34 days curing time.

Fig. 8 depicts C_2 parameter for one of the step-by-step loading–unloading cycles performed in the lowest load range tested. As usual in this work, each impedance measurement has been performed about 20 s after loading; i.e., after reaching the steady state once the various transient phenomena occurring on loading have vanished [21]. It can be seen that some hysteresis remains even at this low level of applied load, thus it seems that elastic and plastic deformations are closely linked, the dominant one depending on applied load (amplitude and frequency), microstructure of the cement paste and water content. Water molecules released on loading seem to have difficulties in being re-adsorbed and allocated in the C–S–H gel interlaminar spaces so leading to a progressive loss of mechanical properties.

Assuming the Kelvin model for the cement paste viscoelastic behaviour with two non-dissipative elements and one dissipative, the fast elastic response (20 s, see

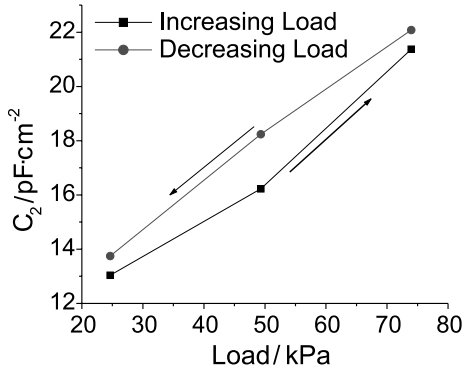

Fig. 8. Variation of C_2 parameter on a loading–unloading cycle for a 0.47 cm thick sample after 34 days hardening. The total loading–unloading cycle takes 2 min.

[21]) will be due to the non-dissipative element not coupled to the dissipative one, while the "slow" response (as corresponding to the compliance cycle depicted in Fig. 8 which takes about 2 min) will be due to the time constant corresponding to the parallel association of dissipative and non-dissipative elements. The dissipative element corresponds to the plastic (creep) behaviour. Formally, the complex compliance corresponds to Eq. (2), if the dissipative element is associated to R and the non-dissipative to C [15]. Thus, information on R can be obtained either at high frequency (as it is the case in Fig. 8) or low frequency (as in traditional creeping tests lasting for weeks [19]).

4. Conclusions and concluding remarks

The above-discussed results allow differentiating two main groups of remarks:

(a) Concerning the microstructure of hardened cement paste. The information contained in complex dielectric constant measurements is closely related to cement paste microstructure. The capacitance C_1 has been related to the solid phase contribution, and the time constant R_2C_2 to the free electrolyte filling the pores. Either τ_2 or its components C_2 and R_2 can be employed as very sensitive parameters to follow on real time structural changes on hardened cement paste induced by loading (namely creeping under constant load and fatigue under cyclical loading).
(b) Concerning corrosion of embedded rebars. The discussed water motion from and to the interlaminar spaces shall affect structures submitted to loading–unloading processes. This periodical presence of free water (electrolyte) shall be equivalent (with respect to the corrosion behaviour of embedded rebars) to wet/dry cyclic tests, which are known as the most aggressive ones due that high oxygen level and water availability are guaranteed. This will be a matter of further studies.

Acknowledgements

The authors thank the Spanish program DGICYT/FEDER for providing financial support to this research under project Ref. 1FD97-1161.

References

[1] Calleja J. New techniques in the study of setting and hardening of hydraulic materials. Am Concr Inst 1952;23:525–36.
[2] McCarter WJ, Brousseau R. The a.c. response of hardened cement paste. Cem Concr Res 1990;20:900–81.
[3] Andrade C, Soler L, Nóvoa XR. Advances in electrochemical impedance measurements in reinforced concrete. Mater Sci Forum 1995;192–194:843–56.
[4] Gu P, Xie P, Fu Y, Beaudoin JJ. A.C. impedance phenomena in hydrating cement systems: frequency dispersion angle and pore size distribution. Cem Concr Res 1994;24:86–8.
[5] Christensen BJ, Coverdale RT, Olson RA, Ford SJ, Garboczi EJ, Jennings HM, et al. Impedance spectroscopy of hydrating cement-based materials: measurement, interpretation, and application. J Am Ceram Soc 1994;77:2789–804.
[6] Coverdale RT, Christensen BJ, Olson RA, Mason TO, Jennings HM, Garboczi EJ. Interpretation of the impedance spectroscopy of cement paste via computer modelling. Part II. Dielectric response. J Mater Sci 1994;29:4984–92.
[7] Coverdale RT, Christensen BJ, Jennings HM, Bentz DP, Garboczi EJ. Interpretation of the impedance spectroscopy of cement paste via computer modelling. Part I. Bulk conductivity and offset resistance. J Mater Sci 1995;30:712–9.
[8] Olson RA, Christensen BJ, Coverdale RT, Ford SJ, Moss GM, Jennings HM, et al. Interpretation of the impedance spectroscopy of cement paste via computer modelling. Part III. Microstructural analysis of frozen cement paste. J Mater Sci 1995;30:5078–86.
[9] Keddam M, Takenouti H, Nóvoa XR, Andrade C, Alonso C. Impedance measurements on cement paste. Cem Concr Res 1997;27:1191–201.
[10] Alonso C, Andrade C, Nóvoa XR, Keddam M, Takenouti H. Study of the dielectric characteristics of cement paste. Mater Sci Forum 1998;289–292:15–28.
[11] Andrade C, Blanco VM, Collazo A, Keddam M, Nóvoa XR, Takenouti H. Cement paste hardening process studied by impedance spectroscopy. Electrochim Acta 1999;44:4313–8.
[12] Cabeza M, Franco M, Izquierdo M, Nóvoa XR, Sánchez I. Effect des chlorures sur les propriétés chimiques et barrière de la pâte de ciment. In: 13ème Forum sur les impedances électrochimiques, Paris, France, 11/12/2000. p. 43–53.
[13] Cabeza M, Merino P, Miranda A, Nóvoa XR, Sánchez I. Impedance spectroscopy study of hardened Portland cement paste. Cem Concr Res 2002;32:881–91.
[14] Diamond S. Mercury porosimetry. An inappropriate method for the measurement of pore size distributions in cement-based materials. Cem Concr Res 2000;30:1517–25.
[15] Havriliak Jr. S, Havriliak SJ. In: Dielectrical and mechanical relaxation in materials. Munich: Hanser Publishers; 1997. p. 1–18.
[16] Cabeza M, Keddam M, Nóvoa XR, Sánchez I, Takenouti H. Dielectric properties and pore structure of hardened Portland cement paste. In: 5th International Symposium on Electrochemical Impedance Spectroscopy (EIS'2001), Marilleva (TN) Italy, 17-22/06/2001. p. 289–90.
[17] Soroka I. In: Portland cement paste and concrete. London: MacMillan; 1979. p. 46–72.
[18] Gani MSJ. In: Cement and concrete. London: Chapman & Hall; 1997. p. 112–6.
[19] Tamtsia BT, Beaudoin JJ. Basic creep of hardened cement paste. A re-examination of the role of water. Cem Concr Res 2000;30:1465–75.
[20] Cao J, Chung DDL. Minor damage of cement mortar during cyclic compression monitored by electrical resistivity measurements. Cem Concr Res 2001;31:1519–21.
[21] Sun M, Liu Q, Li Z, Wang E. Electrical emission in mortar under low compressive loading. Cem Concr Res 2002;32:47–50.
[22] McCarter WJ. The fractal surface of cementitious materials determined by impedance spectroscopy. Adv Cem Res 1994;6(24):147–54.